Functionalized Silicon: A Nanometallurgical Approach to Produce Nanoporous Silicon

Patrick Aggrey, Alexei I. Salimon, and Alexander M. Korsunsky, *Member, IAENG*

Abstract — **Functionalization of silicon has become an interesting research topic due to the excellent combination of properties of functionalized Silicon that could be used in many applications, e.g. in energy conversion based on its good thermoelectric properties. One type of functionalized silicon is its nanoporous form that can be produced by subtractive or additive manufacturing at the nanoscale. However, due to the high cost, the search for cost efficient technologies is currently under way. One promising route is offered by Metallothermic Reduction Reaction (MRR) from silica. Here we report the characterization of nanoporous Silicon produced from diatomite earth via Magnesiothermic Reduction Reaction. The methods used include Raman Spectroscopy, Scanning Electron Microscopy and X-ray Diffraction.**

Index Terms — **Nanoporous Silicon, Magnesiothermic reduction reaction, X-ray Diffraction, Diatomite, Calcination, Raman Spectroscopy**

I. INTRODUCTION

Nanoporous silicon has attracted a lot of attention due to its possible applications in energy harvesting, drug delivery, energy storage, and optical materials [1-6]. Metallurgical silicon has already proven to be very useful in the electronic industry. The metallurgical grade of silicon is however produced at high temperatures, above 1700˚C, making this route unsuitable for producing nanoporous silicon. Cost effective routes of producing nanostructured silicon have been actively sought in recent years.

The use of lower temperatures which in any case lie below the melting temperature of silicon is crucial for this task. Metallothermic reduction reactions have shown a remarkable potential to produce nanostructured Silicon from Silica. Several groups have reported such reactions involving Magnesium, Aluminium, Calcium, as well as a mixture of Al and Mg. Although thermodynamically all reactions are feasible ($\Delta G(Ca) = -168.5$ kJ/mol, $\Delta G(Mg) = -135.9$ kJ/mol, and $\Delta G(Ca) = -157.8$ kJ/mol), the attempt to achieve reduction using Calcium was reported to be unsuccessful [7]. This was attributed to the larger size of Ca atoms which have a relatively high diffusion barrier. Magnesiothermic reduction reactions have been reported to take place between 600 – 700˚C. The onset temperature for the reaction is known to depend on the source of silica, and is reported to be between 400 and 500˚C. It has also been reported that reduction involving Mg may result in the collapse of the nanostructure within silica. Reaction by-products must also be evaluated, as they may affect the performance of the resulting material.

In this paper we report Magnesiothermic Reduction Reaction of diatomite earth using different molar ratios and reduction temperatures, and analyse the resulting variation in the morphology and composition arising from different reaction parameters.

II. MATERIALS AND METHODS

In this paper we report Magnesiothermic Reduction Reaction of diatomite earth using different molar ratios and reduction temperatures, and analyse the resulting variation in the morphology and composition arising from different reaction parameters. Materials and methods

A. *Sample Preparation*

Due to the very exothermic nature of metallothermic reactions, a heat scavenger needs to be used while preparing powder mixture for the reduction. NaCl was selected as the heat scavenger for the Magnesiothermic Reduction Reaction, as reported by Luo et al [8]. The reducing conditions were a reduction temperature of 700˚C, and the molar ratio of SiO_2 and Mg of 1:0.5. The following steps were followed:

- Diatomite earth was mixed with aqueous NaCl solution in the ratio 1:10. The mixture was well stirred using magnetic stirrers at 70˚C.
- The solution was centrifuged and the slurry dried at 85˚C overnight.
- The obtained powder was mixed with magnesium powder in the ratio of 1:0.5.

B. *Magnesiothermic Reduction Reaction*

The Magnesiothermic reduction reaction of diatomite was performed in Argon filled electric furnace. The powder was loaded in an open quartz crucible and reduced at 700˚C. The entire reduction time was 3 hours. The system was heated up to 700˚C and soaked for an hour. The colour of the as-reduced sample changed to coffee brown. The as-reduced sample was first rinsed in deionized water to wash away NaCl. After that it was etched with 1.0M HCl and 5% HF severally.

Manuscript received March 27, 2019; revised April 4, 2019.
This work was supported by Skolkovo Institute of Technology (Skoltech) through Center for Energy Science and Technology (CEST).

P. Aggrey is doctoral student at CEST, Bolshoy Boulevard 30, bld. 1. Moscow, Russia 121205 (e-mail: Patrick.Aggrey@skoltech.ru).
A.I. Salimon is Senior Engineer with CEST, Bolshoy Boulevard 30, bld. 1. Moscow, Russia 121205 (e-mail: A.Salimon@skoltech.ru).
A.M. Korsunsky is with CEST, Bolshoy Boulevard 30, bld. 1. Moscow, Russia 121205, on sabbatical leave from the Department of Engineering Science, University of Oxford, Parks Road, Oxford OX1 3PJ, UK (tel. +44 1865 273043, e-mail: alexander.korsunsky@eng.ox.ac.uk).

It was finally rinsed with deionized water and the filtrate dried overnight at 85˚C. The obtained powder was brownish-yellow in colour, which is similar to colours reported in literature for porous silicon [9].

C. *X-ray diffraction Analysis*

The phase composition, and structure of raw diatomite sample and as-reduced silicon were investigated using the Bruker D8 Advance Diffractometer with Cu Kα1 (λ=1.5405980 Å) with a . Diatomite powder from rock sample was found to be amorphous in nature, just as diatomite samples used for the reduction. As reported in the literature, diatomite samples were calcined above 1200˚C to remove impurities. This changes the amorphous silica to crystalline cristoballite.

D. Powder Distribution and Pore Size Measurement

The diameter and the particle size distribution of the sample were measured on the Fritsch Particle Analyzer. The pore size and specific surface area were determined using the Quantachrome Nova 2200e BET porosimeter. Degassing was performed at 200˚C for 1000 minutes. The specific surface area and pore average pore size are shown in the Table 1

E. Microstructural Analysis

Microstructural analysis of raw and reduced diatomite powders was performed on the JEOL JSM-6480LV Scanning Electron Microscope. Secondary electron images with magnification of 1000x were used for analysis.

F. Raman Spectroscopy

Raman spectra were collected at room temperature using DXR2xi Raman Imaging Microscope. The excitation source used was the 532 nm line of an Ar-ion laser.

III. PROCEDURE FOR PAPER SUBMISSION

The phase composition of raw diatomite was investigated using the Bruker D8 diffractometer. Diffraction pattern of diatomite as presented in Figure 1, clearly showing the presence of amorphous silica, which constitutes the main phase. Unlike in literature where crystalline silica was used, raw diatomite which is amorphous in nature was reduced.

Raw diatomite was as well calcined in air and Argon. While both showed the presence of cristoballite as indicated in Figure 7, they exhibited different colour changes after calcination as shown in Figure 3. Diatomite calcined in Argon changed from brown to copper brown, whereas a red coloured diatomite sample

was obtained after calcination in air. Also, their LOI were almost the same under the different conditions of air and Ar. In Figure 8, the diffraction pattern of as-reduced diatomite is shown. In addition to the elemental Si formed and the remainder of unreacted Silica, a by-product in the form of MgO was also formed. Post-treatment of as-reduced diatomite was necessary to wash away all by-products, NaCl, and unreacted Silica.

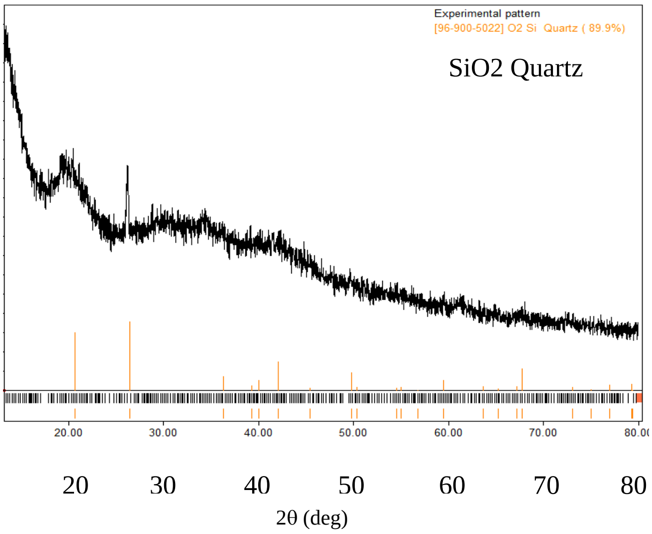

Fig. 1 X-ray diffraction pattern of raw diatomite

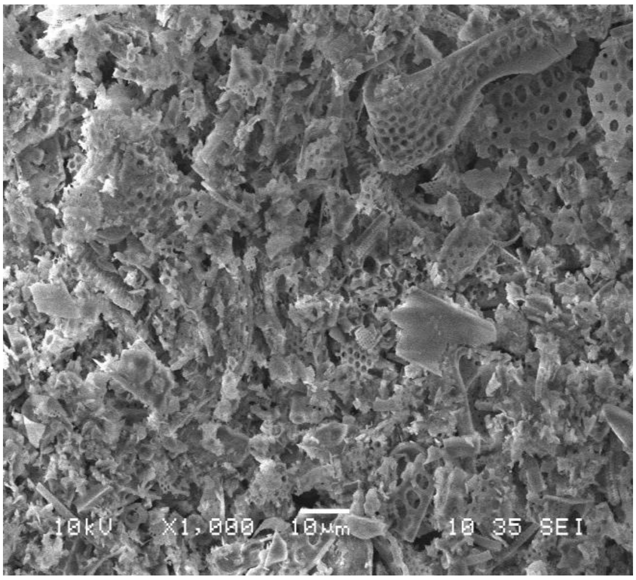

Fig. 2 SEM image of raw diatomite

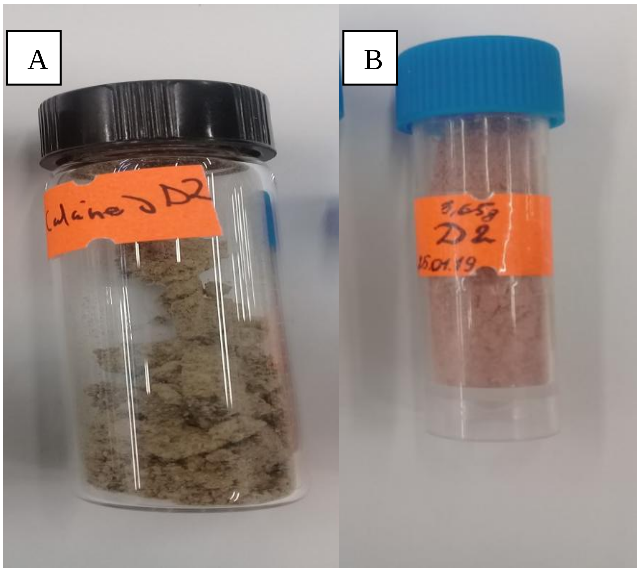

Fig. 3 Colour changes under different calcination condition A) diatomite calcined under flow of Argon B) diatomite calcined in Air

This is confirmed in Figure 9 where peaks of NaCl and MgO are absent. However, due to difficulties in removing Silica by etching, some traces of this component remained.

The diatomite powder had 90 % of particles with size up to ~ 40 µm. In Table 1, the surface area and pore size of the raw diatomite powder are presented. The microstructural analysis of raw diatomite powder also shows the presence of pores which are almost circular in shape, as shown in Figure 2. Due to crushing and milling of raw powder, these nanopores are not uniformly distributed as compared diatomite from rock sample shown in Figure 4. For uniformly distributed pores within the nanostructured silicon product, diatomite from rock sample may represent a good precursor.

Raman spectra of the reduced sample also indicated first order and second order Raman peaks at 513cm^{-1} and 925 cm^{-1} as shown in Figure 10. These values can be compared to the first and second order Raman peaks of 522 cm-1 and 916 cm-1 in literature [10]. Table 2 presents results of colour change and change in mass after calcination under different conditions.

TABLE I
SURFACE AREA AND PORE SIZE

Sample	Surface Area m2/g	Average pore size/ nm
Diatomite	24,1365	0,99031

TABLE II
PROPERTIES DIATOMITE CALCINED AT 1200°C UNDER FLOW OF AIR AND ARGON

Diatomite	Change in diatomite
Mass difference in Air	4.000g to 3.650g
Mass difference in Argon	2.7920g to 2.5259g
Colour change in Air	Brown to copper brown colour
Colour change in Argon	Brown to Reddish colour

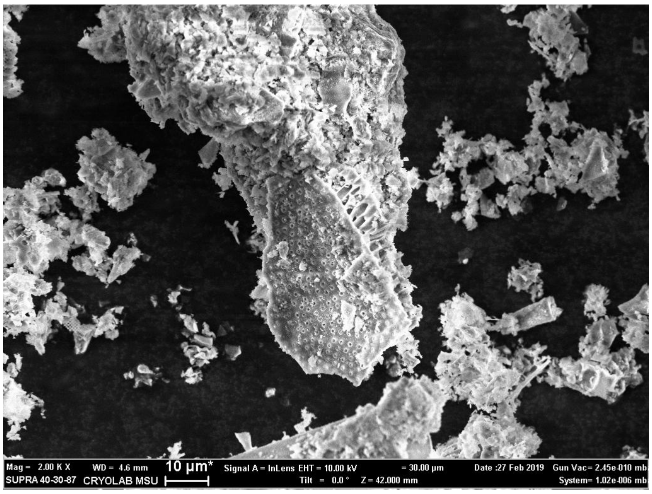

Fig 4 SEM image of diatomite powder from rock sample

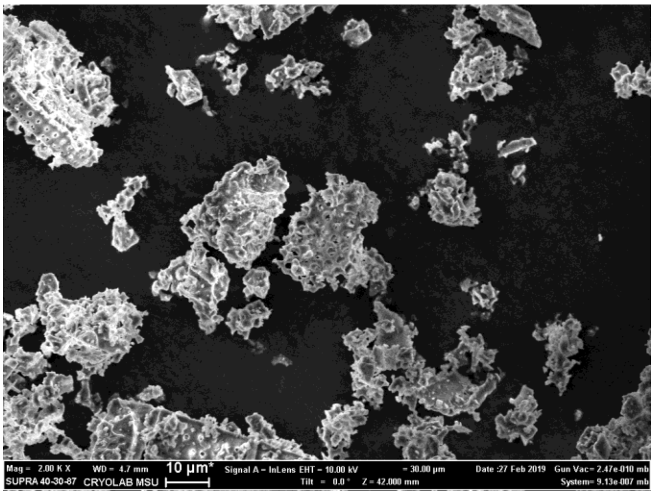

Fig. 5 SEM image of calcined diatomite powder in Air

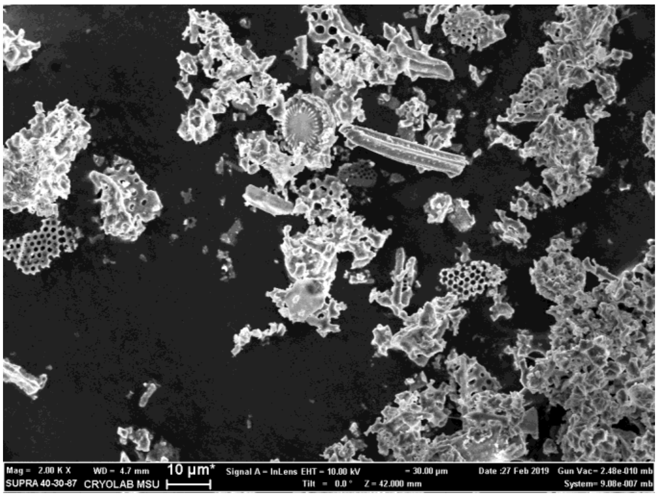

Fig 6 SEM image of calcined diatomite powder under flow of Argon

Also, shown in Figures 5 and 6 are microstructural images of diatomite calcined in air and argon. From Figure 6 it can be seen that the morphology of diatomite calcined in Argon had little morphological damage and hence maintained the internal pores to a greater extent. On the other hand, a fairly collapsed morphology is observed in the diatomite powder that was calcined in air. Diatomite calcined in Argon may be a better precursor for nanoporous Silicon than one calcined in air. Also, volume changes accompanied with phase transformations in silica could have an effect on the morphology of the precursor silica for reduction. Future work will be dedicated to understanding the relationship between the state of raw diatomite powder (calcined or raw), and the morphology of product silicon

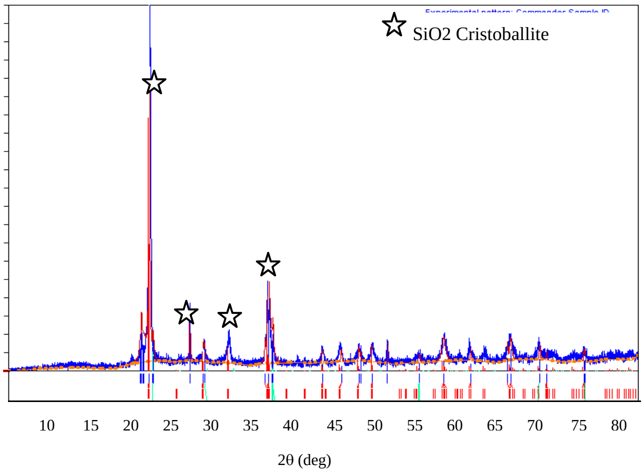

Fig 7 XRD pattern of calcined diatomite powder in Argon

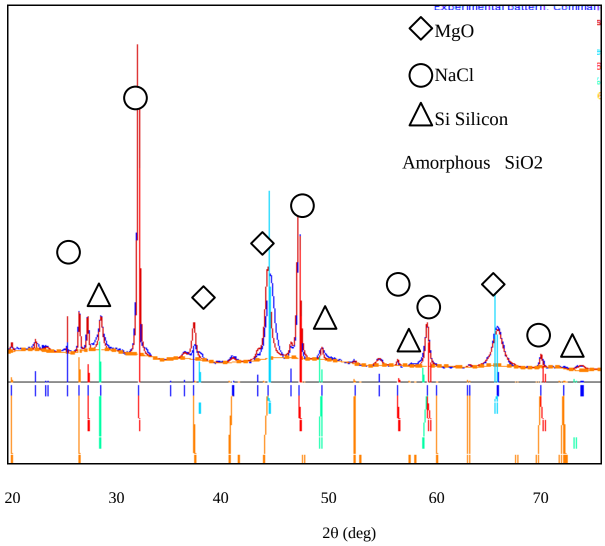

Fig. 8 X-ray diffraction pattern of as-reduced diatomite

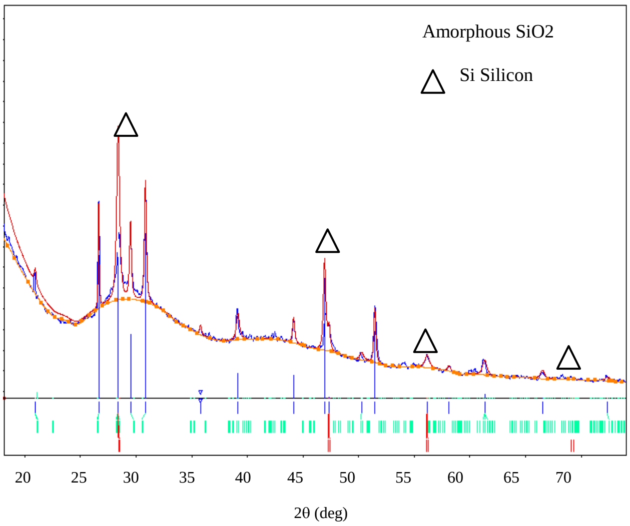

Fig. 9 X-ray diffraction pattern of as-reduced diatomite after etching

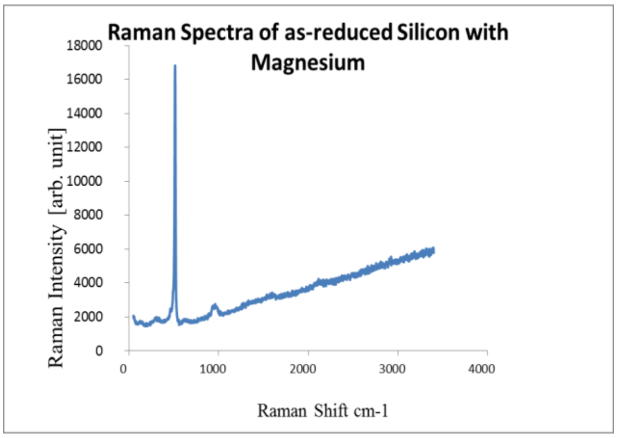

Fig.10 Raman Spectra of Nanostructured silicon from diatomite reduced with Magnesium

IV. CONCLUSION

The powder characteristics of precursor silica (diatomite) were investigated. The effects of different calcination conditions were analysed. Calcination under flow of Argon proved to offer better control over the morphology of calcined diatomite than in air. Elemental silicon was successfully produced from the Magnesiothermic Reduction Reaction of diatomite. Pure elemental silicon could not be retrieved due to difficulties in removing all unreacted Silica by chemical etching. The presence of elemental silicon produced from diatomite via the Magnesiothermic reduction reaction was confirmed by X-ray diffraction analysis and Raman spectroscopy analysis.

ACKNOWLEDGMENT

The authors wish to acknowledge the support from Skolkovo Institute of Technology (Skoltech).

.

REFERENCES

[1] Zong, P. A., Makino, D., Pan, W., Yin, S., Sun, C., Zhang, P., ... & Koumoto, K. (2018). Converting natural diatomite into nanoporous silicon for eco-friendly thermoelectric energy conversion. *Materials & Design*, *154*, 246-253.

[2] Lai, Y., Thompson, J. R., & Dasog, M. (2018). Metallothermic Reduction of Silica Nanoparticles to Porous Silicon for Drug Delivery Using New and Existing Reductants. *Chemistry–A European Journal*.

[3] Entwistle, J., Rennie, A., & Patwardhan, S. (2018). A review of magnesiothermic reduction of silica to porous silicon for lithium-ion battery applications and beyond. *Journal of Materials Chemistry A*, *6*(38), 18344-18356..

[4] Krueger, N. A., Holsteen, A. L., Kang, S. K., Ocier, C. R., Zhou, W., Mensing, G., ... & Braun, P. V. (2016). Porous silicon gradient refractive index micro-optics. *Nano letters*, *16*(12), 7402-7407..

[5] Ocier, C. R., Krueger, N. A., Zhou, W., & Braun, P. V. (2017). Tunable Visibly Transparent Optics Derived from Porous Silicon. *ACS Photonics*, *4*(4), 909-914.

[6] Torres-Costa, V., & Martin-Palma, R. J. (2010). Application of nanostructured porous silicon in the field of optics. A review. Journal of materials science, 45(11), 2823-2838.

[7] Lai, Y., Thompson, J. R., & Dasog, M. (2018). Metallothermic Reduction of Silica Nanoparticles to Porous Silicon for Drug Delivery Using New and Existing Reductants. *Chemistry–A European Journal*, *24*(31), 7913-7920.

[8] Luo, W., Wang, X., Meyers, C., Wannenmacher, N., Sirisaksoontorn, W., Lerner, M. M., & Ji, X. (2013). Efficient fabrication of nanoporous Si and Si/Ge enabled by a heat scavenger in magnesiothermic reactions. Scientific reports, 3, 2222.

[9] Canham, L. (Ed.). (2014). *Handbook of porous silicon* (pp. 163-170). Basel, Switzerland:: Springer International Publishing.

[10] Meier, C., Lüttjohann, S., Kravets, V. G., Nienhaus, H., Lorke, A., & Wiggers, H. (2006). Raman properties of silicon nanoparticles. *Physica E: Low-dimensional Systems and Nanostructures*, *32*(1-2), 155-158.